Mon. Not. R. Astron. Soc. **000**, 000–000 (0000) Printed 10 June 2013 (MN LATEX style file v2.2)

Rotation effects on the Lyman-α line morphology in distant galaxies

Nicolas Garavito-Camargo[1], Jaime E. Forero-Romero[1] and Mark Dijkstra[2]

[1] *Departamento de Física, Universidad de los Andes, Cra. 1 No. 18A-10, Edificio Ip, Bogotá, Colombia*
[2]

10 June 2013

ABSTRACT

Rotation is present in the gas kinematics of galaxies up to the highest redshifts. In this paper we present for the first time radiative transfer calculations that show the impact of rotation on the morphology of the Lyman α line. To this end we construct simplified models where a galaxy is modeled as an homogeneous sphere composed as an homogeneous mixture of dust and hydrogen at a constant temperature. These spheres have a solid-body rotation with linear velocities at the surface in the range $0-300$ km s^{-1}. We consider radiation sources both in the center of the rotating cloud and also homogeneously distributed around the sphere. We find that higher rotational velocities increase the width of each peak in the outgoing line profile while it also increases the amount of Lyman alpha photons escaping in the line center. This trends makes that for high rotational velocities and large Hydrogen optical depths the double peak of the line tends to be erased an be replaced by a single peak the lines center. This is more pronounced for radiation sources homogeneously distributed. Concerning the escape fraction we find that rotation does not have any effect, provided that all the sources are centrally emitted. However in the case of homogeneously emitted sources we measure an increase of about a factor of 2 in the escape fraction for higher rotational velocity values. Our work shows clearly that gas rotation has a non negligible impact on the shape of the Lyman α line.

Key words: galaxies: high-redshift - galaxies: star formation - line: formation

1 INTRODUCTION

Due to the resonant nature of the Lyman alpha line, gas kinematics play an important role shaping its morphology...

There is an extensive literature studying the influence of outflow/inflow configurations in the shape of the outgoing Lyman-alpha line...

In this paper we study for the first time the impact of rotation on the morphology of the Lyman α line. To isolate the effects of rotation we focus on a simple system: the gas distribution is spherical, with homogeneous density and the gas rotates as a solid body. We base our work on two independent Monte Carlo based radiative transfer codes CLARA (**?**) and XX (**?**).

This paper is paper is structured as follows...

In this paper we express a photon's frequency in terms of the dimensionless variable $x \equiv (\nu - \nu_a)/\Delta\nu_\alpha$, where $\nu_\alpha = 2.46 \times 10^{15}$ Hz is the Lyα resonance frequency, $\Delta_\alpha \equiv \nu_\alpha\sqrt{2kT/m_pc^2} \equiv \nu_a v_{\rm th}$ is the doppler broadening of the line which depends on the neutral gas temperature T scattering the radiation or equivalently the thermal velocity $v_{\rm th}$ of the atoms.

2 MODELING BULK GAS ROTATION

Describing the kinematics of gas rotation in all generality is a complex task. There is great variation in the shape of the rotation curve as observed in HI emission as a function of the distance to the galaxy center. However there are two features that are observed very often. First, in the central region the velocity increases proportional to the radius following the behaviour in a body with solid rotation. Second, beyond a certain radius the rotation curve tends to flatten. Furthermore, a thorough observational account of gas rotation in the redshifts of interest for the study of LAEs ($z > 1.0$) is still missing.

An ab-initio description of realistic rotation curves in simulations depends on having access to the dynamic evoluction the mass components in the galaxy: stars, gas and dark matter. Such level of realism is extremely complex to achive, specially of one wants to get a systematic description based on statistics of simulated objects.

Following the tradition of studies of Lymanα emitting systems, we implement a model with a simplified geoemtry and gas distribution. We assume that the gas is homoge-

Physical Parameter (units)	Symbol	Values
Velocity (km s^{-1})	$V_{\rm max}$	0, 50, 100, 200, 300
Hydrogen Optical Depth	τ_H	10^5, 10^6, 10^7
Dust Optical Depth	τ_a	0,1
Photons Distributions		Central, Homogeneous

Table 1. List of the physical parameters that define the spherical models we have simulated using Monte Carlo calculations. For each parameter we vary the values in the range listed in the last column. Takig into account all the possible combinations we end up with 60 different models.

neously distributed in a sphere that rotates as a solid body with constant angular velocity. This simple model will contain only one parameter: the linear velocity at the sphere's surface, $V_{\rm max}$.

2.1 Detailed Implementation of Rotation

In the MonteCarlo code we define a cartesian coordinate system to define the position of each photon. The origin of this system coincides withthe center of the sphere and the rotation axis is defined to be z-axis. With this choice, the components of the gas bulk velocity field, $\vec{v} = v_x\hat{i}+v_y\hat{j}+v_z\hat{k}$, can be written as

$$v_x = -\frac{y}{R}V_{\rm max}, \tag{1a}$$

$$v_y = \frac{x}{R}V_{\rm max}, \tag{1b}$$

$$v_z = 0, \tag{1c}$$

where R is the radius of the sphere and $V_{\rm max}$ is the linear velocity at the sphere's surface. The minus/plus sign in the x/y-component of the velocity indicates the direction of rotation. In this case we take the angular velocity in the same direction as the $\hat{k}$ unit vector. With these definitions we can write the angular velocity as $\omega = V_{\rm max}/R$.

In contrast with spherically symmetric models (static, outflow, inflow) the rotation now defines a preferred direction in the problem. In Section 3 we quantify this differences by varying the line of sight of a mock observer with respect to the rotation axis. The results are parameterized by the polar angle θ as defined by the dot product $\cos\theta = \hat{u}\cdot\hat{k}$.

2.2 Grid of Simulated Galaxies

In the Monte Carlo calculations we follow the propagation of $N_\gamma = 10^5$ numerical photons through different spherical galaxies, each one varying in at least one of the following parameters: the maximum rotational velocity $V_{\rm max}$, hydrogen optical depth τ_H, dust optical depth τ_a and the initial disitrbution of photons with respect to the gas. There are in total 60 models with the input parameters summarized in Table 1.

3 RESULTS

The central result of this paper is summarized in Fig. 1 that shows clearly the considerable impact of rotation on the morphology of the emergent Lyα line. Both panels in the Figure focus on the results for $\tau_H = 10^7$, showing that the influence of rotation is present both when the photons are either homogeneusly or centrally initialized over the gas volume.

In the following subsections we characterize the line morphology by the half-width at half intensity and the peak maxima. In order to intepret the morphological changes in the line we also report the median number of scatter for each Lyα photon in the simulation. Finally we measure the bulk escape fraction as a function of rotational velocity in the presence of dust.

All the results in this section are constructed by taking into account all outgoing photons regardless of the direction of propagation. In the next section **??** we quantify the changes in the observed spectra for observers with different viewing angles.

3.1 Line width and peak maxima

The first quantitative conclusion of the effect of rotation in the Lyα line is that double peaks broaden and reduce their intensity, while the line center rises. This procudes the impresion that, as the rotational velocity increases, the double peaks are merged into a single broad emission peak. This is msot evident in the highest rotational velocities for the homogeneously distributed sources (right panel in Fig. 1).

To quantify the line broadening we measure a modified version of the full width at half maximum (FWHM). Instead we measure it only for half of the line, $W_{1/2}$. This definition allows us to quantify the line width both in the cases of double and single peak emission. In the case of double peaked emission $W_{1/2}$ corresponds to the width of a single peak, while in the extreme case of high rotational velocities, when the double peak is erased, it simply correspond to half FWHM.

Figure 2 shows how $W_{1/2}$ increases with rotational velocity. Continous (dashed) lines connect the results for homogeneous (central) source distribution. The line width increases with rotational velocity up to factors of ~ 2 at 300 km s^{-1}with respect to the static case. For the temperature $T = 10^4$K used in our radiative transfer calculations calculations the thermal velocity is $v_{th} = 12.8$ km s^{-1}. For a model with τ_H it means that the half-width can increase up to 350 km s^{-1}(at $V_{\rm max} = 300$ km s^{-1}) compared to a half-width of 150 km s^{-1}in the static case.

Figure 3 shows the position for the peak maxima as a function of the rotational velocity $V_{\rm max}$. This figure shows us clearly that in the case of central distributed sources there is barely any change with rotational velocity in the range of explored parameters. However, in the case of homogeneously emitted sources the maxima position remain close to constant until beyond some velocity threshold the line becomes single peaked with $x_{\rm max} = 0$.

It is probable that the transition to a single peak line occurs for systems where it becomes easier for the bulk of the photons to escape with the lowest number of scatterings possible, allowing them not to move very far from the center of the line. This hypothesis can help to explain how the single peak stage is easily achieved in the homogeneous source distribution. In this case there is a fraction of the photons that are inside a photosphere region with $\tau_{H,r} \ll \tau_H$

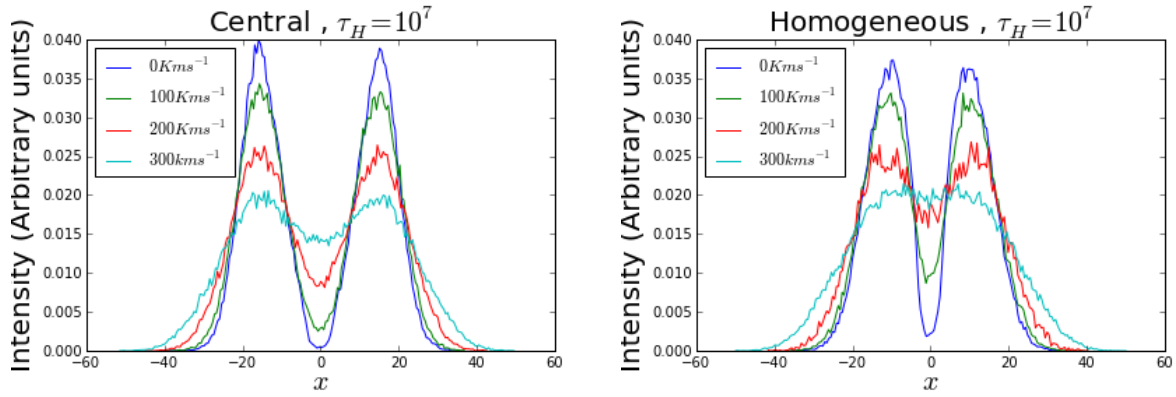

Figure 1. Shape of the Lyα line for different velocities rotational velocities for spherical distributions with $\tau_H = 10^7$. The left (right) panel shows the central (homogeneous) photon distribution. All photons were taken into account regardless of their propagation direction.

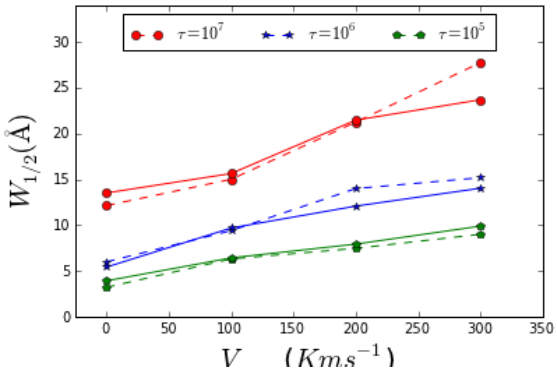

Figure 2. Half-width for the non-dusty models as a function of rotational velocity $V_{\rm max}$. Continous (dashed) lines correspond to homogeneous (central) source distributions.

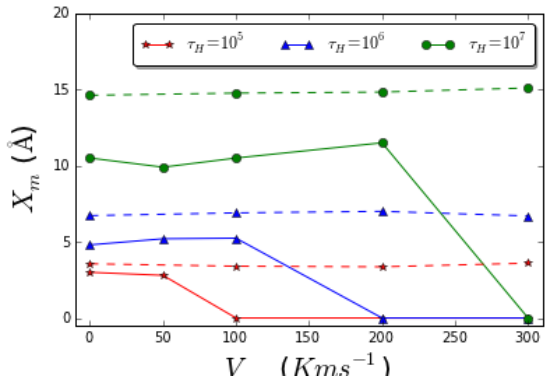

Figure 3. Position of the peak maxima as a function of rotational velocity $V_{\rm max}$. Continous (dashed) lines correspond to homogeneous (central) source distributions. A value of $x_{\rm max} = 0$ indicates that line becomes single peaked.

where $\tau_{H,r}$ is the optical depth from the radius of emission to the sphere's surface. This conditions allows the photons to escape with much less scatterings compared to the photons emitted at the very center of the sphere. In turn, it gives the photons less scatterings to be placed far from the line center. Increasing the rotational velocity $V_{\rm max}$ reduces the optical depth making the photosphere region effectively larger, increasing the number of photons escaping close to the lines's center. For the central case the photosphere is not present, and other mechanisms must be at play in the steady reduction of the double peak.

For larger values of τ_H the transitional velocity $V_{\rm trans}$ is also larger. In our models we find the following correspondance between the optical depth $\tau_{\rm H} = \{10^5, 10^6, 10^7\}$ and the transitional velocities $V_{\rm trans} = \{50 - 100\,{\rm km\ s^{-1}}, 100 - 200\,{\rm km\ s^{-1}}, 200 - 300\,{\rm km\ s^{-1}}\}$ which can only be constrained to be in the range of velocities in the models that gave a $x_{\rm max} \neq 0$ and $x_{\rm max} = 0$. In the next section explore the origin of this trends and consider to what extent the hypothesis of a low number of scatterings is correlated with the emergence of a single peak.

3.2 Average Number of Scatterings

The number of times that a Lyα photon is absorbed and re-emmited is connected to the final frequency that it can have after escaping the galaxy. In the case of static gas geometries, a large value of the optical depth is immediatly followed by a high number of scatterings. In turn a large optical depth increases the probability that a Lymanα photon will be found far from the center of the line. The peak maxima shifting away form the line center as the amount of neutral hydrogen increases.

In Figure 4 we see the average number of scatterings $\langle N_{\rm scatt}\rangle$ as a function of the rotational velocity $V_{\rm max}$. For the central distributions we find that there is not a significante change for increasing rotational velocities, $\langle N_{\rm scatt}\rangle$ changes less than 0.5% for different velocities. In this case we also find that the average number of scatterings is proportional to the optical depth, as expected in analogy from the analytic result for the homogeneous infinite-slab $\langle N_{\rm scatt}\rangle = 1.612\tau_{\rm H}$ (**??**). In our experiments we find $\langle N_{\rm scatt}\rangle = XXX\tau_{\rm H}$.

However, for the homogeneous distribution there is a clear decrease of $\langle N_{\rm scatt}\rangle$ as the $V_{\rm max}$ increases. This effect more pronounced for the lower values of the optical depth. For $\tau_{\rm H} = 10^5$ the average number of scatterings decreases

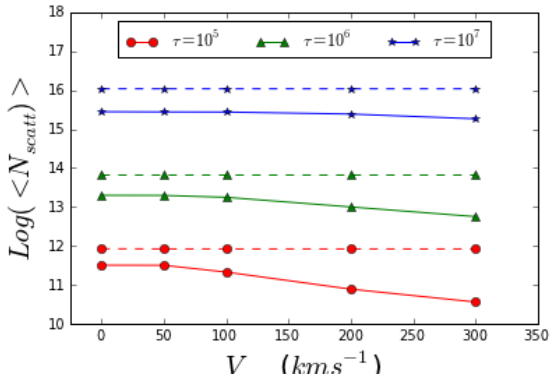

Figure 4. Log of the Average number of scatterings of the outgoing photons as function of the velocity.

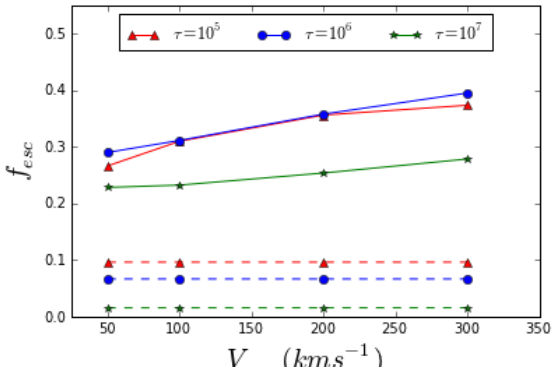

Figure 7. Escape fraction for all the models. continious lines represent the homogenous models, while dashed lines represent the central models

by $XX\%$ at $V_{\rm max} = 300\,{\rm km\ s^{-1}}$ in comparison to the static case.

The analytic expectation for the slab with homogeneously emitted sources is $\langle N_{\rm scatt}\rangle = 1.16\tau_{\rm H}$ (**?**), a factor of 0.72 lower than the case of the centrally emitted photons. In our case we find that for the static spheres this factor is XXX.

In order to understand the effects of rotation in the morphology of the line we make histograms of $< N_{scatt} >$ in function of X_m for both the central Fig. **??** and the homogeneous distribution Fig. 6. For the central distribution and for lower velocities we found that for some value (put the value) of N_{scatt} the mayority of photons have a defined value of X_m. While for higher velocities photons tend spread out in X_m(Make position analysis of this photons).

For the homogeneous distribution we found the same effect but also, for highest velocities the mayority of the photons near the surface escape with much less scatterings that in the static case. This analysis let us conclude that rotation make photons escape with less scatterings and it spread out the wavelenght of the of the outgoing photons represented by X_m.

3.3 Escape Fraction

Until now we have studied models in absence of dust, but is known (REFERENCE) that there is presence of dust in high redshift galaxies. Our models with dust are treated as is explained in detail in the appendix of (Forero et al 2011).

Of particular interest is to compute the escape fraction of Lyman α photons coming from the most distant galaxies, due to the fact that with the observed intensity of the Lyman alpha line quantities as the LF and SFR can be derived (put some references).

Previous studies have shown the correlation of the Escape fraction with galactic mass (Laursen et al 2009, Dayal et al 2010) abundances and the kinematics of dust. In order to study pure rotational effects in the escape fraction we fixed the dust abundance $\tau_A = 0.01$ and the galaxy mass. We compute the escape fraction for the models described in Table 1.

For a realistic model we also take into account the viewing angle, first we fixed the viewing angle at $\theta = 0$ Fig. 7 and then we fixed the velocity in order to see the escape fraction correlation with the viewing angle. Therefore we define the escape fraction as:

$$F_e = \frac{\Sigma_{NI}\vec{k}\cdot\vec{o}}{\Sigma_{NF}\vec{k}\cdot\vec{o}} \tag{2}$$

Where NI is the initial number of photons and NF is the final, $\vec{k}$ is the rotation axis direction and o the observer direction. With this definition we compute the escape fraction for all of our models, the results are presented in Fig 7

In Figure 7 we found that in the central distribution the escape fraction does not change with velocity while it does in the optical depth (See Verhamme 2006, an argument about this). On the other hand for the homogeneous distribution we found that for higher velocities photons escape easily. The difference between this two results rely in the fact that in the homogeneous distribution photons are emitted closer to the escape surface and this makes this configuration more sensitive to rotation while in the central configuration the escape fraction depends mainly in the amount of gas rather than in rotation.

As a final test we compare our results with the analytical solution of the slab developed by (Neufeld 1990) Fig. 3.5, as the geometry we use is different from the one described for Neufeld, we dont expect the same results, in fact we found that for the homogenous sphere the escape fraction is higer than the slab (see ref, mark). Also we notest that for $\tau < 10^6$ the escape fraction does not increase as it will be expected, This is due to the fact that the condition $a\tau_h >> \tau_d$ in not valid any more.

3.4 The Case of Asymmetric Emission

As we know there is unlikely to find galaxies with radiation sources distributed homogeneously. Most of them are in a clumpy distribution (Laursen et al 2013*) which affected the resulting spectra. In order to study an inhomogeneous distribution we set up a model in which we select certain photons that are placed in a specific place but that are not

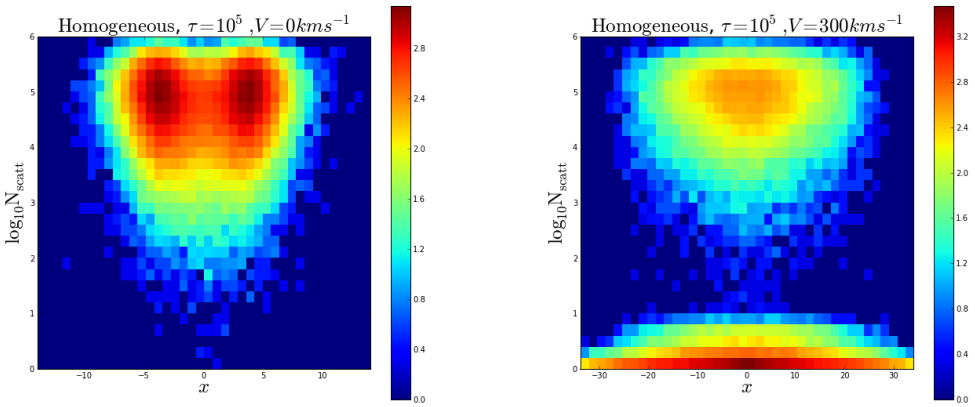

Figure 5. Histogram of N_{scatt} vs x for the homogeneous distribution, left for $V_{max} = 0km/s$, right for $V_{max} = 300km/s$

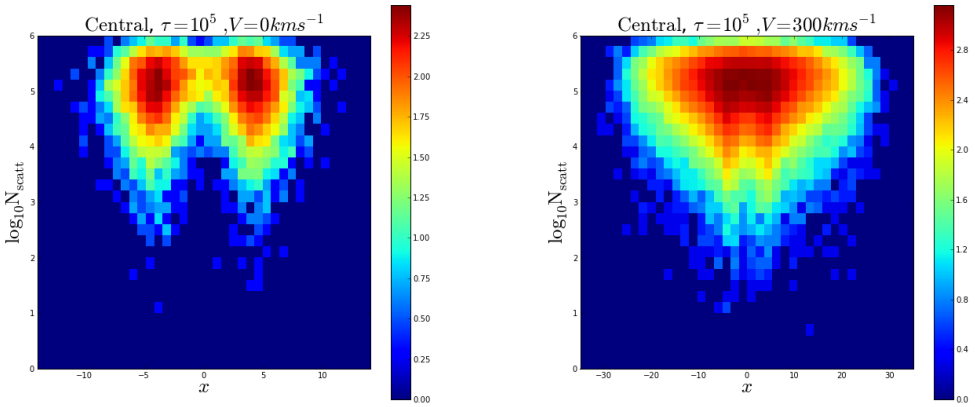

Figure 6. Histogram of N_{scatt} vs x for the Central distribution, left for $V_{max} = 50km/s$, right for $V_{max} = 300km/s$

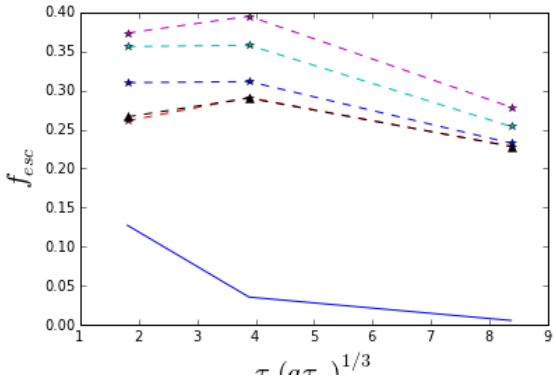

Figure 8. Escape fraction of this work compared with Neufeld analytical solution

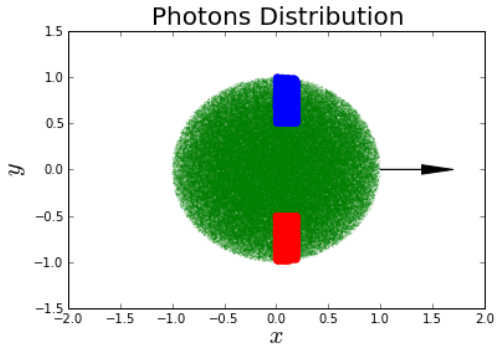

Figure 9. Inhomogeneous distributions of photons, Blue area represents the photons in distribution 1 while red area are the selected photons for distribution 2. The arrow points to the observer position

symmetrically distributed Fig. 9 shows the distributions we set up.

In Fig. 10 we show the resulting spectra of distribution 1 and 2, the first effect we see is the asymmetry of the dou-

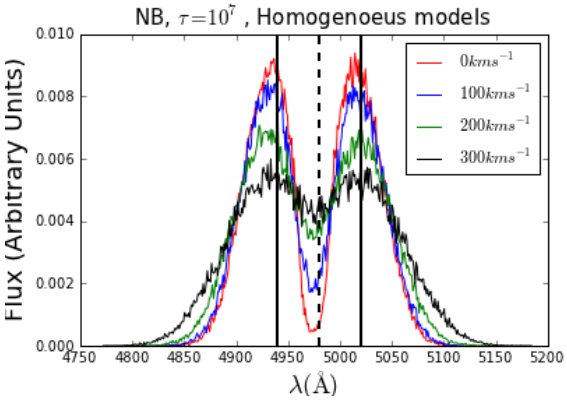

Figure 11. NB filter located at the center of the maxima, with different redshift

ble peak, in the homogeneous and central distribution we see double peaks with the same height, while in this case one peak is higher than the other. For $\tau = 10^5$ we found that in distribution 1 the blueshifted peak is higher than the redshifted, and for distribution 2 the redshifted peak is the highest.

An other important fact here is the asymmetry of the spectra with respect to the line center, in particular photons selected in distribution 1 present a blueshift in their spectra while photons selected in distribution 2 present a redshift. This effect becomes stronger as velocity increase 10

3.5 Integrated flux in a narrowband filter

Until now we have shown the main effects of gas and dust rotation in the Lyα line morphology such as the escape fraction, the FWHM, the maxima position, also we see that shape of the outgoing spectra depends on the position of the observer. It is important to see if rotational effects are detectable in observational methods involving the Lyα line.

One of the most used methods to detect high redshift galaxies using the Lyα line is using a narrowband selection, we make this analysis based on the results obtained by Steidel (2011) in this work (EXPLAIN a lit of bit more about their work) they used tree narrowband filters for tree different redshifts resumed in Table 2, We want to know how much the integrated flux change due to rotational effects in this NB filters, for the models we simulated with CLARA.

In table 2 we present the results of the flux in every narrowband filter for the homogeneous model at different velocities and hydrogen optical depth τ_0. As is well known an increase in the optical depth makes the line peaks separation bigger. In fact for some cases the line width is larger than the NB filer width fig.(put ref fig) for those cases we modify the redshift in the available range in order to make the peak maxima match the NB filter center. For all cases we found that as velocity increase the flux is less.

In the case of the dusty model we found the same trend of the flux with the velocity but in this cases the effect is no that strong. We also found some dependency with the viewing angle.

4 DISCUSSION

... Comparison with Verhamme et al. results on the rotation ... Compare with Kulas et al (Figure 3), Rotation on the lyman alpha line convert double peak profiles into a single one. comments about rotation with inflows and outflows.

... The results derived in this paper have consequences on the interpretation of galaxy observations in the Lyman alpha line. ..compare steidel et al (2011)

5 CONCLUSIONS

In this paper we have estimated the effects of gas bulk rotation on the emission of the Lyman α line. We based the study on the study of a simplified configuration of an homogeneous sphere rotating as a solid body. We explored a range of models by varying the rotation speed, hydrogen optical depth, dust optical depth and initial distribution of Lyα photons with respect to the gas density. This was implemented in CLARA, a Monte-Carlo radiative transfer code already used to study the Lyman α line.

As first we see how the width of the line changes using a modified FWHM explained in section 3.1, and we found that as gas bulk rotation increase also the width increase in a factor of $2-3$ in comparison with the static case. We also take into account the influence of the observer viewing angle, we found that observers with a line of sight perpendicular to the axis of rotation measure a 15% larger line width than those aligned with the rotation axis.

As many observational spectra Lyα emission line (Kulas et al) is double peaked, these peaks provide important information concerning gas kinematics and geometry, which can be partially explained with inflows/outflows of gas content. We study the effect of rotation in the position of this peaks, and we find that the position of the maxima does change with rotation for the homogeneous models when the double peak merged into a single peak as velocity increase. This effect is not seen for the central distribution when the double peak remains constant as the velocity increase. We also find that there is no dependency in the observer viewing angle with the maxima position.

Concerning the escape fraction under rotational effects on the Lyα emission line, we found that the escape fraction increase in about $20\% - 30\%$for the homogeneous sphere model. While rotational effects are negligible for the central models and the escape fraction remains constant. Also the observer viewing angle have no effect in the escape fraction neither for the homogeneous and central models. Complementing this analysis we study the average number of scatterings $< N_{scatt} >$ that photons perform before escaping of the cloud taking into account rotational effects. The main result here is for the homogeneous models for which as velocity increase photons escape with about $\sim 39\%$ less scatterings than in the static case.

As an application of these results we compute the integrated flux taking into account the narrow band filters used by (Steidel et al 2011), for our models we found an important decrease up to 40% for the homogeneous models, and up to 22% for the dusty homogeneous models in the flux as velocity increase. Also we calculate at what redshift should the filter be in order to get the maximum flux, and for the

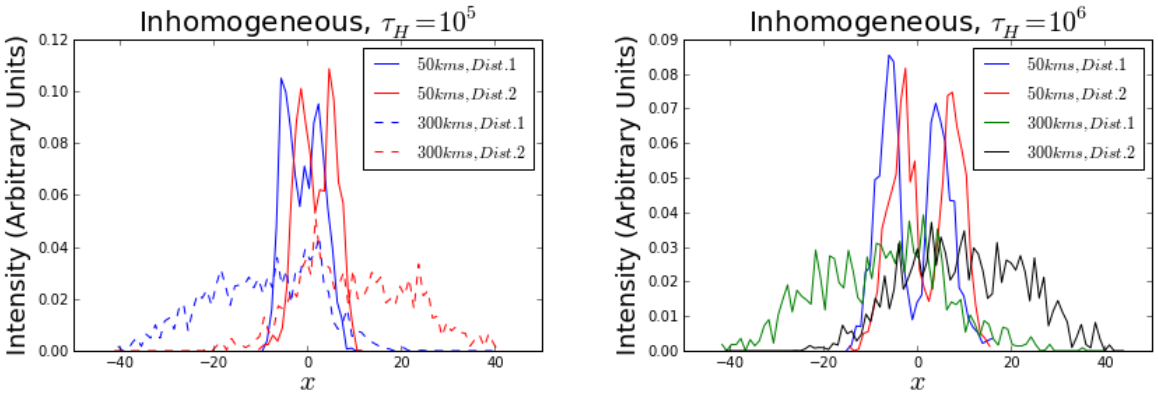

Figure 10. Inhomogeneous model for velocities $50km/s$ and $300km/s$, (left) with $\tau = 10^5$, (right) with $\tau = 10^6$

Model	SSA22a 4980/80	HS1549 4667/80	HS1700 4018/90

Table 2. Fluxes for tree different narrow band filters.

tree filters we get values that rely in the filter redshift range. This effects would have a relevant implication at the time to find high redshift galaxies.

This paper illustrates for the first time the main effects of rotation in the morphology of the Lyα emission line, we estimate the range of this effects for simplified models.

ACKNOWLEDGEMENTS

APPENDIX A: TABLES